Cashew nut shell biomass: A source for high-performance CO<inf>2</inf>/CH<inf>4</inf> adsorption in activated carbon

Journal of CO2 Utilization 83 (2024) 102799

Contents lists available at ScienceDirect

Journal of CO2 Utilization

journal homepage: www.elsevier.com/locate/jcou

Cashew nut shell biomass: A source for high-performance CO_2/CH_4 adsorption in activated carbon

Óscar Javier Fonseca-Bermúdez [a], Liliana Giraldo [b], Rocío Sierra-Ramírez [a], Jarosław Serafin [c,d,e,*], Bartosz Dziejarski [f,g], Marta Gil Bonillo [c], Ghualm Farid [d,e], Juan Carlos Moreno-Piraján [h,**]

[a] Department of Chemical and Food Engineering, Universidad de Los Andes, Bogotá 111711, Colombia
[b] Department of Chemistry, Universidad Nacional de Colombia, Bogotá 111711, Colombia
[c] Department of Inorganic and Organic Chemistry, Inorganic Chemistry section, University of Barcelona, Martí i Franquès 1-11, Barcelona 08028, Spain
[d] Department of Applied Physics, University of Barcelona, C/Martí i Franquès, 1, Barcelona, Catalunya 08028, Spain
[e] ENPHOCAMAT Group, Institute of Nanoscience and Nanotechnology (IN2UB), University of Barcelona, C/ Martí i Franquès, 1, Barcelona, Catalunya 08028, Spain
[f] Faculty of Environmental Engineering, Wroclaw University of Science and Technology, Wroclaw 50-370, Poland
[g] Department of Space, Earth and Environment, Division of Energy Technology, Chalmers University of Technology, Gothenburg SE-412 96, Sweden
[h] Department of Chemistry, Research Group on Porous Solids and Calorimetry, Universidad de Los Andes, Bogotá 111711, Colombia

ARTICLE INFO

Keywords:
Biomass waste
Cashew nut shells
Chemical activation
Activated carbon
CO_2 and CH_4 adsorption
Gas selectivity

ABSTRACT

This study embarks on the synthesis of activated carbon (AC) from cashew nut shells using a potassium carbonate (K_2CO_3) activation process, with a specific focus on its practical application in high-pressure gas adsorption. Among the synthesized samples, MCAK85 emerged as the most efficient, demonstrating a specific surface area of 1693 m^2/g and total and micropore volumes of 0.839 cm^3/g and 0.641 cm^3/g, respectively. Importantly, this bioorganic activated carbon exhibited high sorption capacities for CO_2 and CH_4, with uptake values of 11.0 mmol/g and 5.5 mmol/g at 10 bar at 25°C, and a CO_2/CH_4 selectivity range between 9.1 and 1.8. A comprehensive range of characterization techniques were employed to analyze the structural and chemical properties of the synthesized AC, providing valuable insights into the functional groups and molecular structure. The morphology of the AC was examined using SEM, while the point of zero charge was determined to understand the surface charge characteristics. Additionally, TGA was utilized to assess the thermal stability and composition of the AC. This study underscores the potential of utilizing agricultural waste, specifically cashew nut shells, in the creation of effective materials for gas storage and purification applications. The high-pressure adsorption capacity of the produced AC, coupled with its sustainable and eco-friendly nature, underscores its suitability for environmental and industrial applications, particularly in areas focusing on greenhouse gas capture and air purification, thereby inspiring further research and development in this field.

1. Introduction

In recent years, the international community has seen a heightened awareness of climate change, promoting increased exploration of technologies aimed at mitigating emissions of greenhouse gasses like CO_2, CH_4, N_2O, and O_3. These gasses contribute significantly to atmospheric contamination and climate change. Especially the rapid surge in global CO_2/CH_4 emissions poses a significant and enduring threat to the natural environment, standing out as the foremost contributor to adverse effects among greenhouse gases over several decades [1]. This persistent trend, a key driver of global warming and climate change, shows no signs of abatement. The substantial increase in atmospheric CH_4 and CO_2 levels, escalating at a rate of 0.17 % annually, can be primarily attributed to the Industrial Revolution. According to estimates by the National Oceanic and Atmospheric Administration [2], the atmosphere contained 421 parts per million (ppm) of CO_2 as of 2022. This

* Corresponding author at: Department of Inorganic and Organic Chemistry, Inorganic Chemistry section, University of Barcelona, Martí i Franquès 1-11, Barcelona 08028, Spain.
** Corresponding author.
E-mail addresses: jaroslaw.serafin@qi.ub.es (J. Serafin), jumoreno@uniandes.edu.co (J.C. Moreno-Piraján).

https://doi.org/10.1016/j.jcou.2024.102799
Received 19 February 2024; Received in revised form 23 April 2024; Accepted 3 May 2024
Available online 16 May 2024

represents a remarkable 50 % elevation compared to pre-industrial levels and an additional 13 % rise since the year 2000. Extensive research underscores that the upward trend in CO_2/CH_4 emission is predominantly a consequence of industrial activities, particularly the combustion of coal and petroleum [3–7]. Industries engaged in petroleum refining, cement production, steel and iron manufacturing, and power plant operations, operate intricate systems with complex processes and demands. These activities collectively exert a severe impact on the climate and temperature of the earth. Despite the challenges posed by CO_2 emissions contributing to climate change and posing threats to human health, there is a pressing need for effective and acceptable solutions, even as green technology may seem ambitious. In the short term, one of the most feasible options to curtail CO_2 emissions is through capture and storage, a consensus supported by the Intergovernmental Panel on Climate Change (IPCC). The IPCC has set an ambitious goal of reducing CO_2 emissions by 50 % by 2050 [8,9].

In recent decades, there has been a concentrated effort to create novel solid materials with the objective of capturing deleterious gases. Among these materials are diverse forms of porous solids, chosen for their remarkable versatility and adaptability. Multiple technologies are available for capturing CO_2 emissions from combustion processes. These methods include absorption, cryogenics, carbonation-calcination cycles, the use of membranes, and adsorption. Notably, adsorption holds a distinct advantage over other techniques due to its superior selectivity and lower energy consumption, contribution to reduced associated production costs. The adsorbents utilized in this context must exhibit a porous structure and favorable surface chemistry. Given the acidic nature of CO_2, it is essential for the surface of the carbonaceous material to be appropriately tailored to enhance selectivity for this contaminant [10,11]. Currently various solids are under investigation for CO_2 adsorption, including activated carbons [12–15], zeolites [16,17], silica [18–20], metal-organic frameworks [21–23], and organic polymers [24].

Activated carbons, known for their porous nature and versatile adsorption capabilities, play a significant role in CO_2 adsorption due to their textural characteristics, high surface area, tunable porosity, high degree of surface reactivity, good stability, and affordable low price for industrial applications [25,26]. Globally, the annual production of activated carbon is estimated to reach approximately 100,000 tons [27, 28]. Predominant sources for commercial-scale activated carbon include wood, anthracite, bitumen charcoal, lignite, peat shell, and coconut. Additionally, alternative sources like olive and almond shells are increasingly being utilized. The carbon content of these materials varies from 40 % to 90 % (wt.), with a density ranging from 0.4 to 1.45 g/m^3, 29, 30,. Efforts have been directed towards leveraging waste as raw materials for activated carbon production [29]. Agricultural residues, such as olive cores, biomass, rice husks, corn stalks, bagasse, fruit stones (cherry and apricot stones, grape seeds), hard shell (pistachio, almond, and pecan shells), fruit pulp, bones, and coffee beans, can also serve as sources [30–33]. The chosen raw material for activated carbon preparation should ideally be abundant, cost-effective, and safe [34,35]. Furthermore, minimizing mineral content and ensuring minimal biodegradability during initial storage are crucial considerations [36]. Cashew (Anacardium occidentale), originating from Brazil, is known for its resilience to pests, soil rejuvenation properties, and low maintenance during cultivation, making it an ideal crop with the potential for low production costs and income opportunities. Major global cashew producers include Vietnam, India, Nigeria, Ivory Coast, Brazil, and Indonesia, with Vietnam leading in exports. In Colombia, cashew cultivation is concentrated in various departments, offering a planting potential of 5,000 to 10,000 ha per year [37]. The cashew industry primarily focuses on processing cashew nuts, which make up 10 % of the fruit. The remaining 90 % is the edible pseudocarp, the cashew apple, widely used for juice production globally. Processing generates a substantial amount of shells, comprising 50–65 % of raw nuts. In Colombia, inadequate waste treatment for cashew shells poses environmental risks, with direct deposition in open fields and potential contamination of water reservoirs. The Vichada region, a significant player in the Colombian cashew market, faces challenges in managing agricultural by-products, as evidenced by the processing of 5.2 tons of raw nuts in 2021, yielding only 1.4 tons of the desired commercial product [38]. This issue highlights the need for effective waste management practices in the cashew industry.

In this work, we convert an important biomass waste of post-industrial production into activated carbon using chemical activation with K_2CO_3. Its physicochemical properties were tested via different characterization techniques (N_2/CO_2 isotherm, FT-IR/Raman spectroscopy, SEM, TGA, and PZC), and it was used as a potential sorbent for CO_2 and CH_4 high-pressure adsorption, as well as its selectivity. This research not only contributes to the field of waste management by providing a novel method to repurpose industrial biomass waste but also offers insights into developing effective solutions for gas adsorption, crucial for addressing environmental challenges.

2. Methodology

2.1. Preparation of activated carbons

The cashew nut shells (CNS) were obtained from Puerto Carreño (Vichada) province of Colombia. The CNS were stored at −4 °C before undergoing grinding. The frozen CNS were grounded using a blade mill with a 4 mm mesh. Then, a 50 % w/w solution of K_2CO_3 was used to impregnate the CNS. The impregnation ratio is 1:1 (activated carbon: activating agent), and the impregnation was conducted at a temperature of 85 °C while stirring for 3 hours. After this period, the temperature was raised to 150 °C, and the material was dried. The impregnated and dried materials underwent thermal treatment in a tubular furnace under an inert nitrogen atmosphere (150 mL/min), where potential reactions could occur according to Eqs. 1–3. The activation process was carried out at three different temperatures: 800 °C, 850 °C, and 900 °C (MCAK80, MCAK85 and MCAK90). The activation temperature is maintained for three hours, and the heating ramp is set at 5 °C/min. The activated carbons obtained undergoes multiple washing cycles until the pH of the washing water remains constant. Finally, the activated carbons were dried for 24 hours in a convection oven, as shown in Fig. 1.

$$\text{Biomass} + 2\,K_2CO_3 \rightarrow \text{Activated Carbon} + CO_2 + H_2O + \text{Other Products} \quad (1)$$

$$\text{Activated Carbon} \rightarrow \text{Heat Carbonization} \quad (2)$$

$$\text{Carbon} + K_2CO_3 \rightarrow \text{Activated Carbon} + CO_2 + K_2O \quad (3)$$

Additionally, the above reaction can be explored in more details as below:

Decomposition of potassium carbonate:

$$K_2CO_3 \rightarrow K_2O + CO_2 \quad (4)$$

This initial step involves the thermal decomposition of potassium carbonate (K_2CO_3) at elevated temperatures. The decomposition yields potassium oxide (K_2O) and carbon dioxide (CO_2) as products. Further, interaction with carbonaceous precursor occurs:

$$K_2O + C \rightarrow 2\,K + CO \quad (5)$$

This reaction is crucial for the activation process as it initiates the development of porosity in the carbon structure. Ultimately, the formation of active sites and pore development take place:

Potassium oxide reacts with carbon, resulting in the formation of carbon dioxide and the regeneration of potassium carbonate:

$$K_2CO_3 + C \leftrightarrow K_2O + CO \quad (6)$$

$$K_2O + C \leftrightarrow 2\,K + CO \quad (7)$$

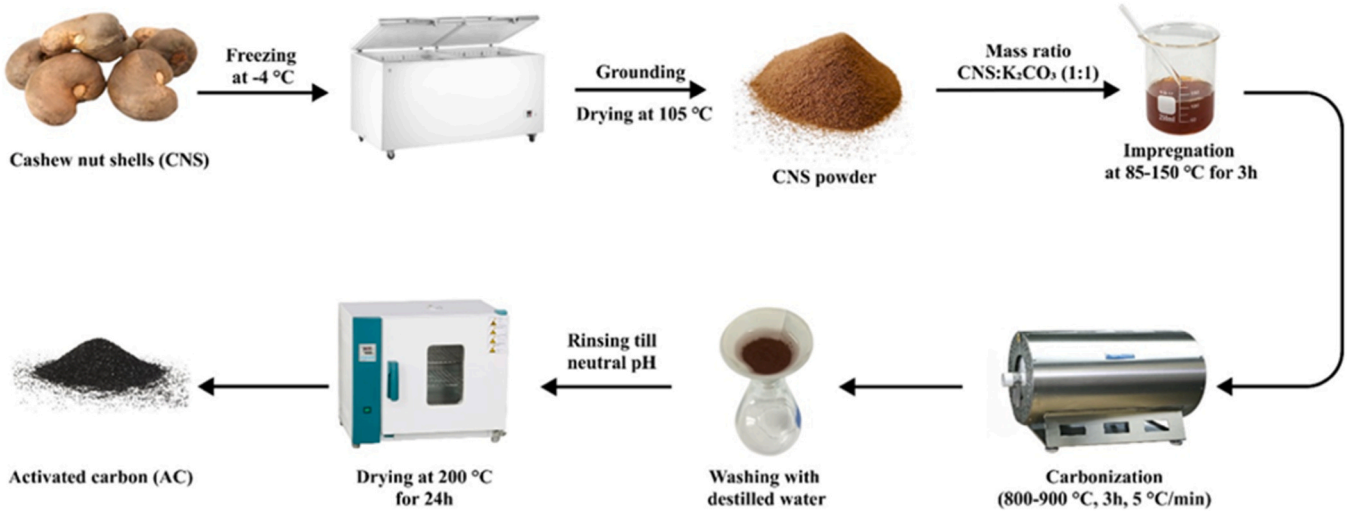

Fig. 1. Schematic preparation of activated carbon derived from cashew nut shells.

$$2K + CO \leftrightarrow K2O + CO \quad (8)$$

This sequence of reactions drives the conversion of potassium carbonate (K_2CO_3) and carbon (C) into various products under neutral conditions, promoting the formation of porous carbon structures with high surface activity [39].

2.2. Characterization of carbon-based materials

The thermogravimetric analysis technique is employed to assess the weight loss and thermal effects experienced by the CNS during pyrolysis under an inert atmosphere. Approximately 10–20 mg of the sample is taken and subjected to heating at a rate of 10 °C/min until reaching a temperature of 900°C. The heating process is conducted with a nitrogen flow of 100 mL/min using an STA 7200 Hitachi High-Tech instrument equipped with the TAT 81 7200 standard analysis software. The structure of activated carbon is examined using the scanning electron microscopy (SEM) technique with the JSM 6490-LV JEOL microscope. Fourier transform infrared spectroscopy (FT-IR) is employed to identify functional groups in the activated carbon. The Thermo Scientific Nicolet 6700 equipment is utilized, scanning in the range of 400–4000 cm^{-1}. The sample is prepared with KBr, forming a tablet with a solid-KBr ratio of 0.1 %. Raman spectroscopy is performed using the Xplora model dispersive Raman spectrometer from Horiba Scientific. The instrument is equipped with a confocal microscope and three laser excitation lines at wavelengths of 514 nm, 632 nm, and 785 nm. The resulting Raman spectra are detected by a CCD detector. The point of zero charge values of each activated carbon were measured by preparing solutions adjusted to a range of 3–11 pH units by adding appropriate amounts of 0.1 M HCl and 0.1 M NaOH. Then, 0.5 g of the adsorbent sample is added to 50 mL of each solution. After 72 hours of stirring at room temperature, the final pH value is measured.

To determine the textural properties of the solids investigated in this study, nitrogen adsorption-desorption isotherms are conducted at a temperature of −196°C. Approximately 0.1 g of carbonaceous samples are subjected to degassing at 250°C for several hours using a Micromeritics ASAP 2020 equipment. The BET method is employed to calculate the specific surface area. The volume of micropores is assessed using the Dubinin-Astakhov method. The pore size distribution is calculated based on the NLDFT model. In addition, volumes of micropores (<1.4 nm) and narrow micropores (<0.7 nm) were calculated with CO_2 (99.99 % pure) adsorption at 0 °C.

High pressure adsorption isotherms were carried out in the ASAP 2050 sorption analyzer from Micromeritics. This equipment is designed to reach high pressures (greater than 15 bar). The hydrogen adsorption was carried out up to 10 bars at a temperature of 77 K. The high-pressure adsorption isotherms of CO_2 and CH_4 were measured up to 10 bars at a temperature of 298 K.

3. Results and discussion

3.1. Textural properties

Fig. 2 shows the N_2 adsorption isotherms depicted in the dataset exhibit a distinctive Type I profile, indicative of the microporous nature of the material under investigation. This type of isotherm is characterized by a rapid and steep initial nitrogen uptake at low relative pressures, signifying the efficient filling of micropores. Such behavior aligns with materials possessing well-defined microporous structures, where the majority of adsorption occurs within the micropore volume [40]. Moreover, observation is the presence of a very small H4-type hysteresis loop in the isotherm. The H4 hysteresis loop is associated with slit-shaped pores, reflecting a narrow range of pore sizes. Although relatively rare, the occurrence of H4 hysteresis indicates a specific type of mesoporosity, namely, slit-like mesopores [41]. The steep ascent in

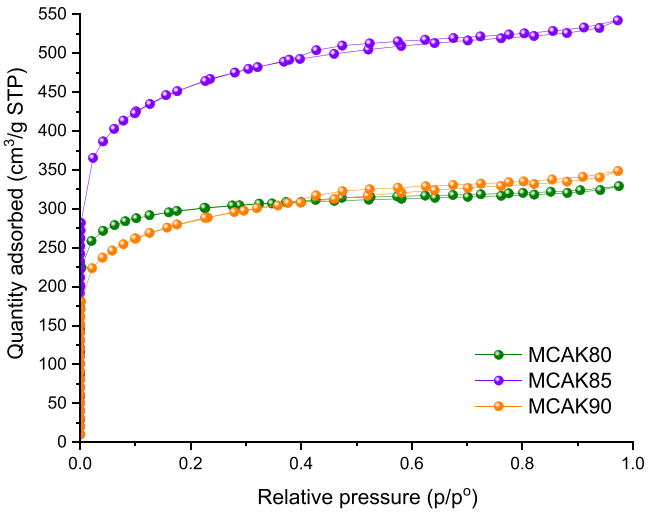

Fig. 2. Nitrogen isotherms for carbon samples activated at 800°C, 850°C and 900°C.

adsorption at low relative pressures, in conjunction with the Type I isotherm, underscores the material's efficient and swift nitrogen adsorption within the microporous structure. This characteristic is particularly desirable for applications requiring high microporosity, such as in gas storage or separation processes. The very small H4-type hysteresis loop suggests the presence of a limited range of slit-like mesopores, contributing to the overall adsorption capacity in a controlled manner. The coexistence of the Type I isotherm and the very small H4-type hysteresis loop signifies a dual porosity characteristic. The material primarily exhibits microporosity, characterized by efficient adsorption within micropores, while also featuring a limited range of slit-like mesopores. This combination positions the material as a compelling candidate for applications demanding precise control over CO_2 and CH_4 gas adsorption, including gas storage and selective gas separation processes [42,43].

Table 1 shows the textural properties of carbon samples subjected to diverse activation temperatures (800°C, 850°C, and 900°C), providing profound insights into their suitability for gas sorption applications, particularly emphasizing the adsorption of CO_2 and CH_4. The activation temperature plays a pivotal role in shaping the porosity of the carbon material, influencing its gas sorption capabilities. The specific surface area (S_{BET}), a fundamental metric indicating available surface for gas adsorption, underscores a significant divergence among the samples. Notably, the material activated at 850°C exhibits a substantial increase in S_{BET} (1693 m^2/g) compared to its counterparts activated at 800°C (1164 m^2/g) and 900°C (1038 m^2/g). In this study, a non-local density functional theory (NLDFT) model was utilized, employing the N_2 and CO_2 adsorption-desorption isotherm at −196 °C and 0 °C, respectively, to ascertain the pore size distributions. Total pore volume (V_{total}), a holistic indicator of space available for gas storage, further substantiates the impact of the activation temperature on pore development. The sample activated at 850°C outperforms others with a V_{total} of 0.839 cm^3/g, highlighting superior gas storage potential compared to those activated at 800°C (0.510 cm^3/g) and 900°C (0.539 cm^3/g). The calcination process at 850°C fosters the creation of a larger pore volume, providing ample space for gas storage. While the average pore size remains consistent across samples, maintaining an average of 1.63 nm, the nuanced impact of activation temperature on microporous volume (Vmicro) is crucial micropores, characterized by their dimensions below 2 nm, play a critical role in high-capacity gas sorption. The 850°C-activated sample has a notably higher Vmicro (0.641 cm^3/g) compared to counterparts activated at 800°C (0.494 cm^3/g) and 900°C (0.397 cm^3/g).

The variation in pore size among the samples activated at different temperatures. It appears that the smaller pore size observed in the sample activated at 900°C compared to those activated at 800°C and 850°C may be attributed to the intensified carbon gasification process at higher temperatures. At elevated temperatures, such as 900°C, the activation process tends to be more vigorous, leading to increased carbon removal through gasification reactions. This enhanced gasification may have resulted in the closure or collapse of larger pores, thereby yielding a material with a smaller average pore size compared to samples activated at lower temperatures. This explanation aligns with the well-established understanding of carbon activation kinetics, where higher temperatures promote more rapid gasification reactions and subsequent pore development. Therefore, it is plausible that the heightened gasification kinetics at 900°C led to the observed reduction in pore size.

Table 1
Textural parameters of the bioorganic prepared activated carbons.

AC sample	S_{BET},m^2/g	V_{TOT},cm^3/g	Pore size,nm	V_{micro},cm^3/g
MCAK80	1164	0.51	1.82	0.494
MCAK85	1693	0.839	1.63	0.641
MCAK90	1038	0.973	1.63	0.397

As can be observed in Fig. 3(a,b), which presents the pore distribution of the volume of micropore diameters the highest peaks are seen around 0.35 nm (narrow micropores <0.7 nm), a part of that is mostly focused between 1 and 1.35 nm, related to the two highest peaks at 1.1 and 1.2 nm for MCAK-850 and one the highest peak at 1.3 nm for MCAK-900; the mesopore diameters are largely centred in the range 2–4 nm. Micropores, owing to their size, offer an ideal environment for efficient adsorption, with CO_2 and CH_4 molecules readily accommodated within these confined spaces. The observed decrease in textural properties for the sample MCAK-900 activated at 900°C may be attributed to intensified carbon gasification processes. At higher temperatures, excessive activation can lead to the over-gasification of the carbon matrix, resulting in a reduction of surface area and pore volume. This phenomenon may be associated with the increased severity of reactions during activation at 900°C, causing a loss of structural integrity and a decrease in porosity. The PSD of ACs below 1 nm arising from kinetic restrictions of N_2 molecules at 77 K was examined with CO_2 adsorption at 273 K [44].

3.2. Fourier-transform infrared spectroscopy (FT-IR)

Fig. 4 shows the comprehensive Fourier-transform infrared (FTIR) analysis conducted on a diverse spectrum of activated carbon matrices has details regarding their chemical composition, particularly in relation to distinct functional groups. This rigorous examination, reliant on the identification of indicative frequencies, has afforded a nuanced understanding of the molecular architecture of the activated carbon samples.

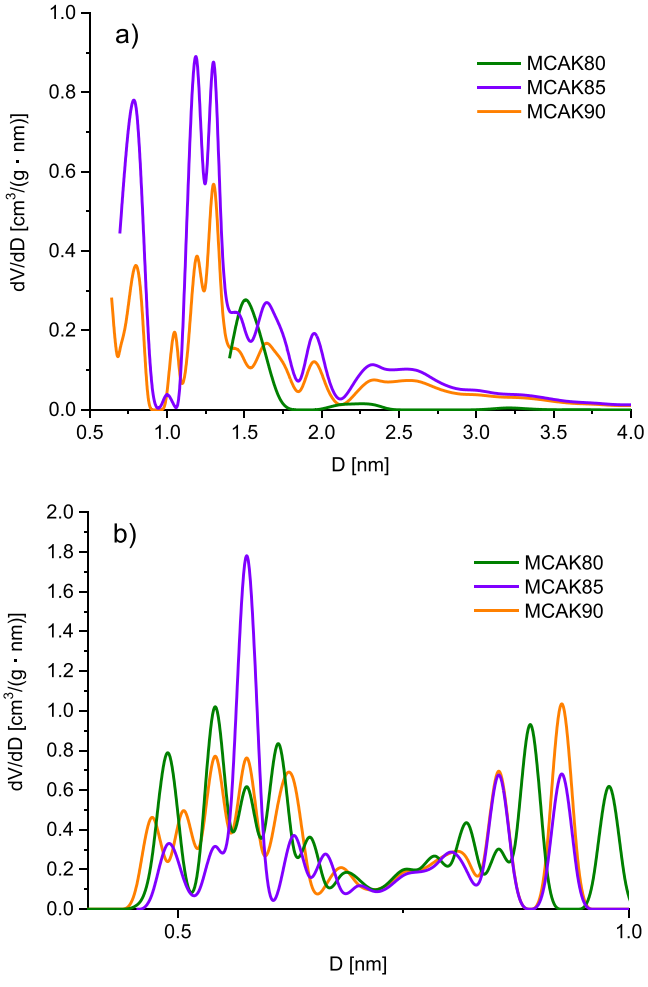

Fig. 3. Pore size distribution determined with the DFT method based on N_2 adsorption isotherm (a) and CO_2 adsorption isotherm (b).

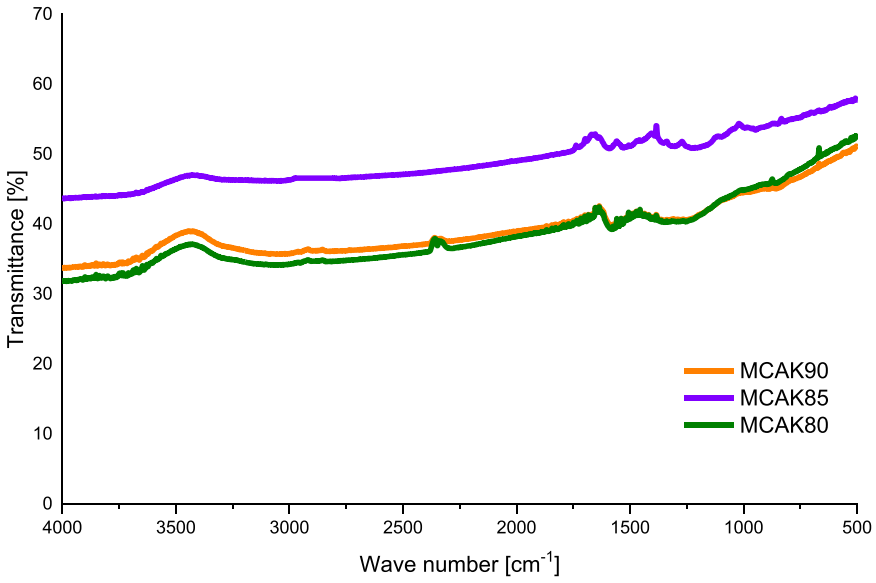

Fig. 4. FTIR spectra for the sample activated at 800°C, 850°C and 900°C.

Within the high-frequency region of 3700–3584 cm^{-1}, the FTIR spectra exhibited a medium peak intensity with sharp characteristics, indicative of the O-H stretching vibration associated with alcohol functional groups [45]. This observation implies the presence of hydroxyl moieties, possibly arising from the thermal treatment during activation or residual oxygen-containing precursors within the biomass source. Transitioning to the mid-frequency range of 1700–1600 cm^{-1}, a medium peak intensity manifested, denoting the C═C bending vibration characteristic of alkene functionalities [46]. This observation suggests the incorporation of unsaturated carbon-carbon bonds, which may have originated from the precursor biomass or undergone transformation during the high-temperature activation process. Further analysis of the spectral data within the range of 1350–1000 cm^{-1} revealed a distinctive stretching vibration corresponding to C-N bonds, indicative of amine functional groups [47].

The presence of amines implies the existence of nitrogen-containing compounds, potentially derived from the original biomass feedstock or introduced during the activation process (Table 2). Upon correlating the indicative frequencies with their corresponding functional groups, a significant revelation emerged. Activated carbon samples subjected to higher activation temperatures, specifically at 800°C and 900°C, exhibited discernible signals associated with alkene and amine compounds. This insight underscores the influence of elevated activation temperatures on the preservation or formation of these functional groups within the activated carbon structure. Remarkably, the sample MCAK-850 processed at 850°C presented a distinct compositional profile characterized predominantly by aromatic compounds. This deduction was made based on the absence of characteristic peaks associated with alkene and amine functionalities. The nuanced variations observed in the activated carbon's molecular architecture at different temperatures underscore the complexity of the activation process and its impact on functional group evolution.

Table 2
Functional groups of activated carbons from CNS.

Absorption (cm^{-1})	Appearance	Group	Compound Class
3700–3584	Medium peak intensity, sharp	O-H Stretching vibration	Alcohol
1700–1600	Medium peak intensity	C═C Bending vibration	Alkene
1350–1000	-	C-N Stretching vibration	Amine

3.3. Raman spectroscopy

Fig. 5 shows the Raman spectra provide a sophisticated spectroscopic fingerprint, allowing for the detailed characterization of carbon bonding configurations within the activated carbon. The D peak, associated with disordered regions, and the G peak, associated with ordered graphitic structures, collectively unveil the intricate interplay of molecular arrangements that define the heterogeneous nature of the material's microstructure. The presented data affords an insight into the microstructural characteristics of the activated carbon samples, elucidated through the discernment of well-defined D and G peaks in their Raman spectra. These distinctive peaks serve as indicative markers of the material's heterogeneous microstructure, where the D peak arises from the vibration of carbon-carbon sp^2 bonds, indicative of disorder or structural irregularities. In contrast, the G peaks result from the vibration of sp^2 carbon bonds within an ordered structure reminiscent of graphite [48]. The degree of graphitization was calculated using the ratio of intensities of the D peak and G peaks where:

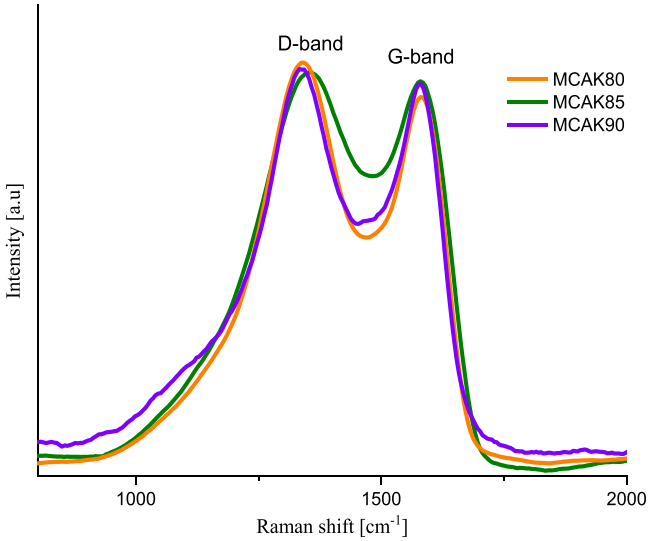

Fig. 5. Raman spectra for the samples activated at 800°C, 850°C and 900°C.

$$R = \frac{I_D}{I_G} \quad (9)$$

R – is the degree of graphitization of carbon materials;
I_D – is the intensity of the D peak;
I_G – is the intensity of the G peak.

The measured frequencies of the D and G peaks, spanning 1330–1400 cm^{-1} and 1580–1600 cm^{-1}, respectively, align closely with reported values in the literature for disordered carbon matrices. This agreement substantiates the credibility of our experimental findings and reinforces the notion of a heterogeneous microstructure prevalent in the activated carbon samples. A more intricate analysis involves the assessment of the degree of disorder within the carbon matrices, quantified through the intensity ratio of the D peak to the G peak (I_D/I_G). Across the spectrum of elaborated activated carbons, this ratio falls within the range of 0.846–0.857. Such a span is recognized by prior studies as characteristic for non-ordered carbon materials (Table 3). Importantly, higher values within this range suggest an augmented presence of aromatic rings and a diminished occurrence of carbon-containing structural defects. This tendency fosters the formation of functional groups on the material's surface, often entailing oxygen atoms.

3.4. Scanning electron microscopy (SEM) analysis

Fig. 6 provides a comprehensive microstructural examination of activated carbon surfaces, using SEM micrographs to unveil intricate details crucial to understanding of the material's adsorption characteristics, particularly in the context of CO_2 and CH_4 adsorption. The micrographs within Fig. 6 disclose discernible microporous networks embedded within the CA structures. Remarkably, these micropores exhibit an absence of clogging by extraneous particles, indicative of a well-defined and open microporous morphology. In the realm of gas adsorption, this observation holds paramount significance, as an unimpeded microporous structure is inherently favorable for facilitating efficient and selective adsorption of CO_2 and CH_4 molecules [49,50]. The lack of pore blockage ensures the uninhibited accessibility of micropore space, thus optimizing the material's adsorption performance by allowing for unencumbered gas-surface interactions. Concurrently, the examination of macroporous surfaces across various AC samples reveals a striking uniformity, notwithstanding differences in activation temperatures during synthesis. This consistent microporous morphology assumes pivotal importance in the realm of gas adsorption applications. Macropores, serving as conduits for gas diffusion, contribute to the accessibility of the inner microporous structure. The observed uniformity implies that activation temperatures, while influencing microstructural features, do not substantially modify the broader macroporous architecture. This steadfast consistency ensures a reliable and reproducible gas adsorption behavior across diverse samples, emphasizing the material's potential for application in gas separation and storage systems. Importantly, it should be emphasized that the considered type of material derived from nut biomass appears to be a worthy contender for the title of high-quality substrate rich in micropores, which has been confirmed in other studies [51–53].

Table 3
Raman D and G peak frequencies and intensities rates I_D/I_G for all activated carbon samples.

Temperature (°C)	D peak frequency (cm^{-1})	G peak frequency (cm^{-1})	I_D/I_G
900	1343.1	1580.4	0.849
850	1349.2	1573.9	0.857
800	1327.1	1568.1	0.846

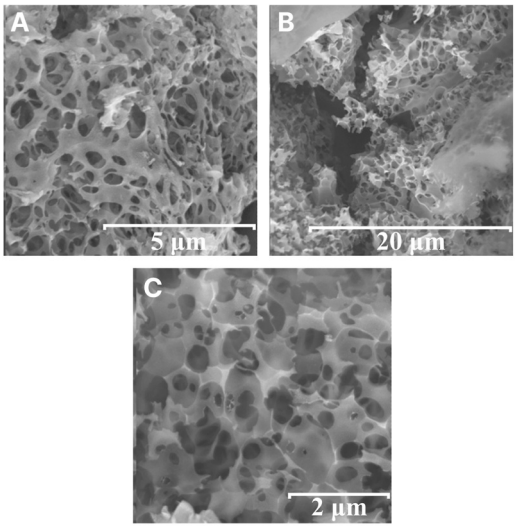

Fig. 6. SEM micrographs A) MCAK800 (5 µm), B) MCAK850 (20 µm), C) MCAK900 (2 µm).

3.5. Point of zero charge (PZC)

The point of zero charge (pHpzc) of an adsorbent is a critical parameter representing the pH at which the material's surface attains a state of electrical neutrality. This concept is pivotal in understanding the electrochemical interactions governing adsorption phenomena. When the pH of the solution designated for adsorption surpasses the pHpzc, the adsorbent's functional groups undergo protonation due to an excess of H+ ions. Conversely, at pH values below the pHpzc, deprotonation occurs as a result of the presence of OH- ions. Furthermore, in situations where the pH of the solution exceeds the pHpzc, yielding negative net charges, a predilection arises for the attraction of cations to the activated carbon matrix. In contrast, at pH values lower than the pHpzc, a competitive environment ensues, driven by the prevalence of H+ ions within the positively charged matrix. This milieu favors the attraction and subsequent adsorption of anions. The specific points of zero charge values for the activated carbon samples (MCAK-800=7.2; MCAK-850=7.3; and MCAK-900=7.6) (Table 4) signify pH conditions at which the surface charge is nearly neutral. This near-neutral pH at the pHpzc implies that the anticipated adsorption behavior of the prepared samples is not significantly influenced by charge-induced attraction effects. The proximity to neutrality at the pHpzc underscores a balanced electrochemical state, indicating that the surface charge of the activated carbon samples plays a limited role in dictating their adsorption characteristics under these conditions [54]. The delineation of pHpzc values offers a nuanced understanding of the electrochemical intricacies governing the adsorption behaviour of activated carbon. This level of detail is crucial for designing and optimizing adsorption processes in gas-phase adsorption, where pH-dependent interactions play a pivotal role in dictating adsorption efficacy [55]. Table 3. pH at the point of zero charge for samples activated at 800°C, 850°C and 900°C.

3.6. Thermogravimetric (TGA) analysis

The thermogravimetric analysis (TGA) of untreated cashew nut shell (CNS) has provided nuanced insights into the intricate thermal decomposition processes inherent to this biomaterial (Fig. 7 and Fig. 8). The

Table 4
Zero Charge values for the activated carbon samples.

Sample's Activation Temperature [°C]	800°C	850°C	900°C
pH Point of Zero Charge	7.2	7.3	7.6

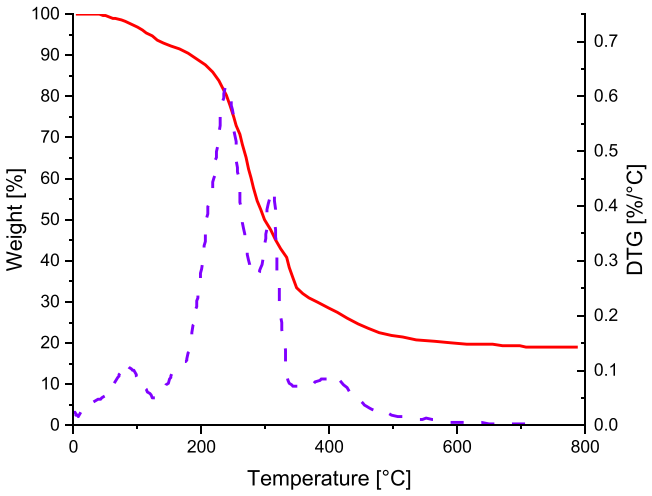

Fig. 7. TGA of raw CNS.

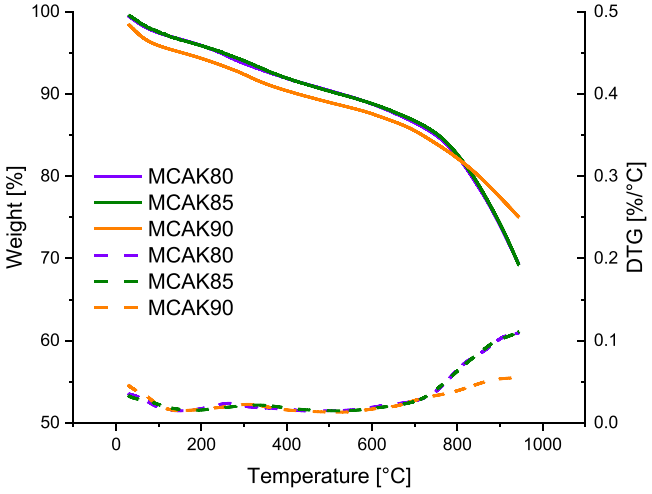

Fig. 8. TGA of activated carbons produced from CNS.

three distinct peaks observed at approximately 250°C, 320°C, and 400°C in the TGA curve signify complex thermal events related to the diverse chemical constituents within CNS. The first decomposition peak at 250°C is specifically associated with the decarboxylation of anacardic acid, a key component found in cashew nut shell liquid (CNSL). Anacardic acid undergoes thermal decomposition, leading to the formation of cardanol [56]. This process is essential to elucidate, as it sheds light on the transformation of a specific bioactive compound under thermal conditions, impacting the potential applications of CNS in various fields. The subsequent decomposition events, occurring in the temperature range of 300–400°C, are attributed to the thermal breakdown of other components present in CNSL, such as cardanol. The identification of these temperature ranges for decomposition is crucial for understanding the stability and behaviour of CNSL constituents under varying thermal conditions, providing fundamental knowledge for applications in pyrolysis or thermal processing. Furthermore, the observation that the solid fraction of CNS, comprising structural carbohydrates like starch and natural fibers, degrades within the same temperature range (300–400°C) underscores the complexity of the CNS matrix [57]. The simultaneous decomposition of these diverse components at similar temperatures necessitates a comprehensive understanding of the thermal dynamics governing each constituent, facilitating tailored approaches for the extraction or processing of specific compounds. The derivative thermogravimetry (DTG) curve reinforces these observations by delineating three principal decomposition steps. The distinctive features of the DTG curve between 250°C and 400°C highlight the thermal events associated with CNSL constituents, providing a finer resolution of the decomposition process. This detailed characterization aids in identifying optimal temperature ranges for the controlled release or extraction of specific CNSL compounds with desired properties. The negligible weight loss observed at temperatures exceeding 500°C suggests that conducting CNS activations at higher temperatures is advisable. This recommendation is grounded in the desire to minimize residual CNSL remnants, which could be undesirable in certain applications. The scientific rationale behind this recommendation lies in the enhanced thermal stability of CNS matrix components at temperatures surpassing 500°C, reducing the likelihood of undesired byproducts and residues. Similar results and conclusions were obtained by Papadopoulou & Chrissafis [58].

3.7. CO_2 and CH_4 high-pressure adsorption

The CO_2 and CH_4 capture capacities of MCAK80, MCAK85, and MCAK90 were examined at 298 K and in the range 0–10 bar. Fig. 9 (a,b) shows a comparative analysis of the performance of activated carbon samples in terms of CO_2 and CH_4 adsorption isotherms. The experimental findings demonstrate that MACK85 has the most significant CO_2 uptake, measuring 11.0 mmol/g at 10 bar, owing to its superior surface area (1693 m^2/g) and micropore volume (0.641 cm^3/g). This illustrates

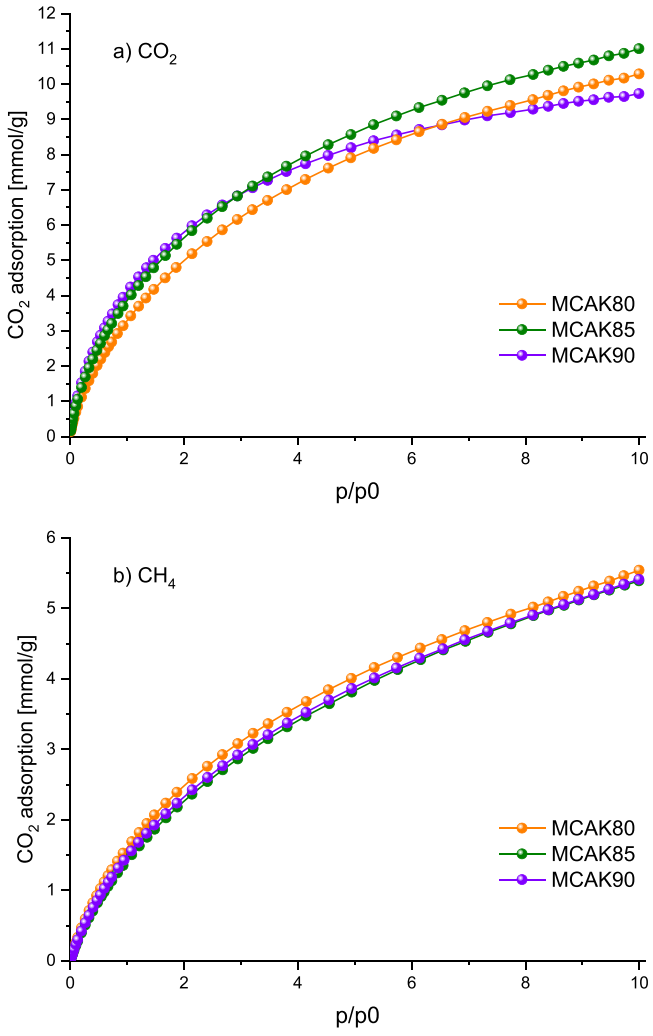

Fig. 9. CO_2 (a) and CH_4 (b) high-pressure isotherms of measured at 25°C in the range of 0–10 bar.

that the presence of microporosity greatly affects the adsorption of CO_2, whereas MCAK85 (0.494 cm^3/g) and MCAK90 (0.397 cm^3/g) exhibits lower CO_2 adsorption capacities, reaching 10.30 and 9.70 mmol/g, respectively. On the other hand, the CH_4 adsorption curves exhibit little divergence, with the only noticeable difference being the variance in CH_4 uptake (5.4–5.5 mmol/g).

The adsorption mechanisms of CO_2 and CH_4 on ACs obtained from biomass can be intricately shaped by the micropore architecture, gas molecular dimensions, and prevailing physical adsorption processes. This intricate interplay is particularly notable under ambient conditions (25°C and pressures reaching up to 10 bar). The micropore configuration within biomass-derived activated carbon, featuring nanoscale dimensions, establishes a comprehensive network of minuscule adsorption sites. Operating at 25°C, the moderate temperature strikes a balance between kinetic factors and thermodynamics. When combined with pressures up to 10 bar, these conditions create a favorable environment for the efficient diffusion of gases into the micropores. The molecular dimensions of CO_2 and CH_4 are pivotal in this adsorption process. CO_2, possessing a smaller molecular diameter of approximately 0.33 nm, readily infiltrates the micropores, participating in physical adsorption driven by van der Waals forces. Similarly, CH_4, with a slightly larger molecular diameter of about 0.38 nm, experiences physical adsorption within the micropores, utilizing van der Waals interactions with the carbon surface [59]. Within the realm of surface functional groups, the activation procedure introduces diverse oxygen-containing moieties, such as hydroxyl (-OH), carbonyl (C═O), and carboxyl (-COOH) groups. Additionally, the inclusion of carbon-carbon double bonds (C═C) and carbon-nitrogen (C-N) groups adds complexity to the adsorption dynamics. C═C groups, renowned for their π-electron cloud, contribute to heightened adsorption, particularly for CO_2, through π-π interactions. Conversely, C-N groups introduce polar characteristics, fostering interactions with both CO_2 and CH_4, thereby influencing the overall adsorption capacity [60,61].

The data presented in this work have been comprehensively compared with findings reported in the relevant literature in Tables 5 and 6.

3.8. Relation of CO_2/CH_4 adsorption with textural properties

The relationship between CO_2/CH_4 adsorption and various textural properties was examined, as given in Fig. 10. This study reveals a notable variation in the correlation between CO_2/CH_4 adsorption capacity and different textural properties of the materials and prove aforementioned assumptions of mechanism. The most significant observation is the strong correlation between adsorption capacity and microporosity, as indicated by the high R^2 values ranging from 0.991 to 0.994. This suggests that microporosity is a critical factor in the adsorption process for these gases. In stark contrast, the correlation with total pore volume is minimal, with an R^2 value of only 0.056, implying that total pore volume might not be a significant determinant in the adsorption efficiency of CO_2 and CH_4 under the conditions tested. The Brunauer-Emmett-Teller (BET) surface area exhibits a moderate correlation, with R_2 values between 0.914 and 0.967, indicating its relevance but not as pronounced as microporosity. These findings contribute to a deeper understanding of the adsorptive behavior of ACs for CO_2/CH_4 capture and storage.

Table 5
CO_2 adsorption capacities for carbon materials presented within the literature.

Precursors	CO_2 adsorption capacity (mmol/g)	Temperature (°C)	Pressure (bar)	References
Cashew nutshell	4.0	25	1	This work
	11.0	25	10	
Cashew nutshell	6.2	0	1	[62]
Arundo donax (Stem)	4.1	0	1	[63]
	21.2	0	30	
Black locust	5.9	0	1	[64]
	3.8	25	1	
Coffee grounds	7.2	0	1	[65]
	4.2	25	1	
	16.4	0	10	
	12.7	25	10	
Coconut shell	5.6	0	1	[66]
	3.9	25	1	
Lignin waste	4.6	25	1	[67]
	17.3	25	20	
Jujun grass & Camellia japonica	5.0	25	1	[68]
	21.1	25	20	
Mesquite wood	6.5	5	3	[69]
	26.0	25	30	

Table 6
CH_4 adsorption capacities for carbon materials presented within the literature.

Precursors	CH_4 adsorption capacity (mmol/g)	Temperature (°C)	Pressure (bar)	References
Cashew nutshell	1.7	25	1	This work
	5.5	25	10	
African palm shell	7.6	25	45	[70]
Coconut shell	7.7	25	40	[71]
Corncob	16.8	25	34.5	[72]
Cornelian cherry stones	2.5	25	1.2	[73]
Damson plum stones	1.4	25	1.2	
Olive stones	13.3	5	35	[74]

3.9. CO_2/CH_4 selectivity studies

The preference of an adsorbent material in selecting CO_2 over CH_4 is crucial for a range of environmental, industrial, and economic considerations in certain industrial uses. Based on the adsorption patterns of CO_2 and CH_4 at 25 °C, an in-depth analysis of the selectivity between CO_2 and CH_4 was carried out. This research involved calculating the gas selectivity of CO_2/CH_4 using the ideal adsorption solution theory (IAST) to precisely estimate the effectiveness of the separation process.

The IAST approach, developed by Myers and Prausnitz, is extensively employed for determining the adsorption selectivity of gas mixtures in porous substances [75]. This integration follows a specific equation of state to provide an accurate assessment.

$$S_{IAST} = \frac{q_{CO_2(p)}}{q_{N_2(p)}} \bullet \frac{p_{CH_4}}{p_{CO_2}} \tag{10}$$

where: S_{IAST} is the selectivity coefficient, $q_{CO2(p)}$ and $q_{CH4(p)}$ refer to the uptake of specific gas [mmol/g], p_{CH4} and p_{CO2} are the partial pressure in the mixture.

As a result, our focus was on investigating the selectivity for a CO^2/CH_4 (0.5/0.5) binary mixture. In this context, Eq. (1) is modified and expressed in the following specific form:

$$S_{IAST(EQ)} = \frac{q_{CO_2(p)}}{q_{CH_4(p)}} \tag{11}$$

Fig. 11 displays the selectivity data derived from IAST for both equimolar and flue gas CO_2/CH_4 mixtures at 25 °C. It's notable that there's a marked decline in the CO_2/CH_4 selectivity ratio for both gas compositions up to a pressure of 0.2 bar. Specifically, the selectivity coefficient of CO_2 relative to CH_4 varied significantly, ranging from 9.1 to 1.8 correlating with a pressure increase from 0.01 to 10 bar.

Table 7 shows the selectivity values for various carbon-based materials as found in existing literature, measured at 10 bar and with an

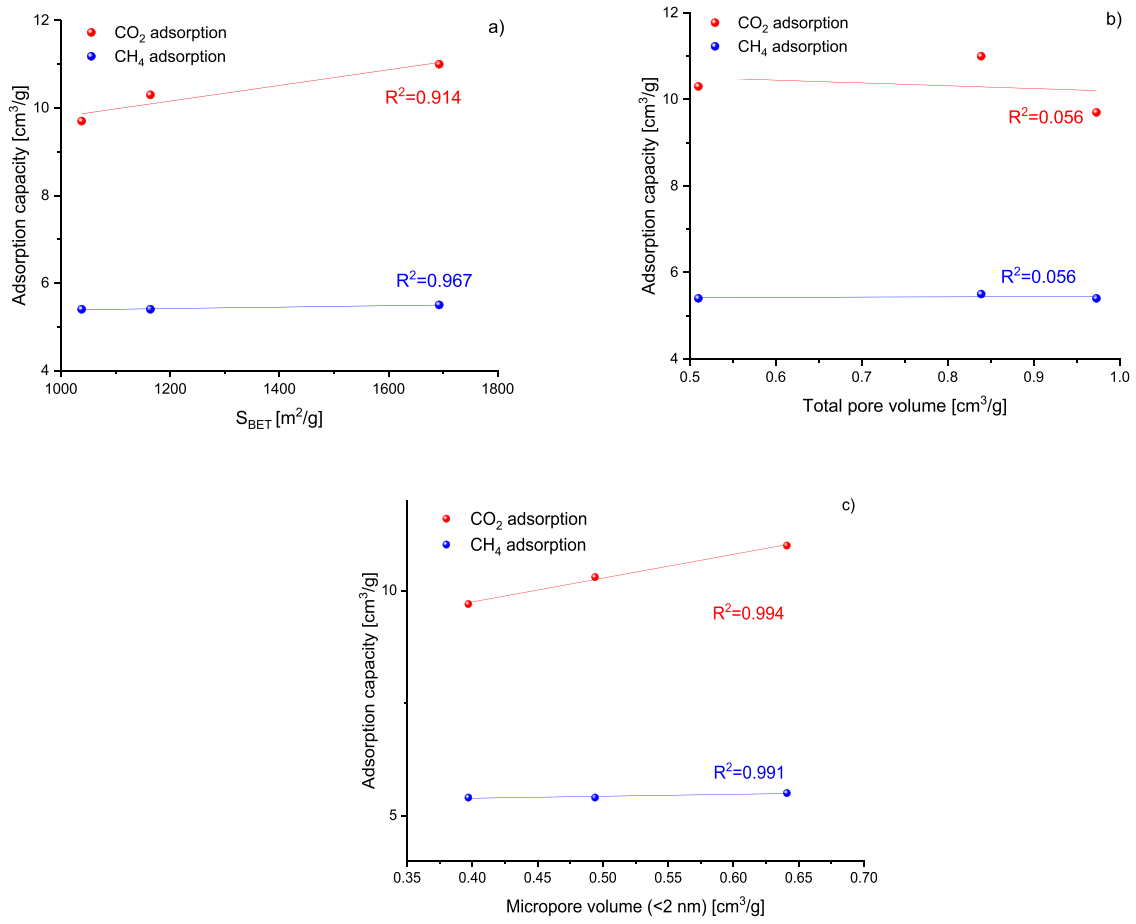

Fig. 10. CO_2/CH_4 adsorption uptake at 25 °C up to 10 bar as a function of (a) BET surface area (b) total pore volume, and (c) micropore volume <2 nm.

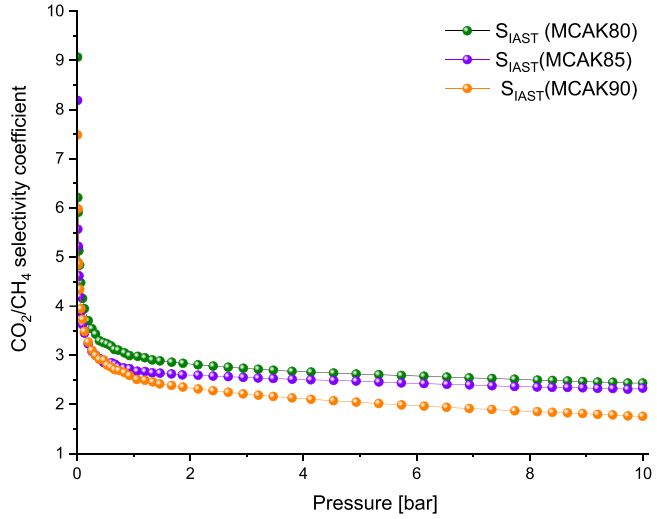

Fig. 11. CO_2/CH_4 selectivity of MCAK samples versus pressure at 25 °C.

initial CO_2 molar concentration approximately around 50 %. The selectivity values achieved in this study are similar to those reported for carbonaceous materials under comparable conditions.

4. Conclusions

In this study, the development and characterization of activated carbon derived from cashew nut shells using a K_2CO_3 activation process is presented. Among the various samples synthesized, the most efficient one, labeled as MCAK85, demonstrated impressive qualities in terms of surface area and pore volume. Specifically, it exhibited a specific surface area of 1693 m^2/g, along with total and micropore volumes of 0.839 cm^3/g and 0.641 cm^3/g respectively. Notably, ACs showcased a remarkable sorption capacity, particularly for CO_2 and CH_4. The CO_2 and CH_4 uptake were at 11.0 mmol/g and 5.5 mmol/g for the MCAK85, respectively, under a pressure of 10 bar at a temperature of 25°C. Furthermore, the material displayed selective adsorption capabilities, with a CO_2/CH_4 selectivity range of 9.1–1.8. The successful utilization of cashew nut shells, a widely available agricultural waste product, in producing high-quality activated carbon, is a significant step towards sustainable and eco-friendly material science. This approach not only adds value to what is typically considered waste but also offers an

Table 7
Comparison of CH_4/CO_2 selectivity of carbonaceous materials at 10 bar.

Material	Selectivity	Temperature (°C)	References
MCAK80	2.4	25	This work
MCAK85	2.3	25	This work
MCAK90	1.8	25	This work
WV1050	5.2	30	[76]
Norit R1	2.7	25	[77]
Honeycomb monoliths	2.0	26	[78]
A35/4	3.4	20	[79]
Ordered mesoporous carbon	3.0	25	[80]
Desorex K43-Na	2.1	25	[81]
GAC 1240	2.7	30	[82]

efficient solution for gas sorption applications. The high performance of the MCAK85 sample in terms of gas uptake and selectivity indicates its potential for practical applications in areas like gas storage, air purification, and perhaps even in tackling environmental challenges such as greenhouse gas capture.

CRediT authorship contribution statement

Óscar Fonseca-Bermúdez: Writing – original draft, Methodology, Investigation, Formal analysis, Data curation. **Marta Gil Bonillo:** Data curation, Writing – original draft. **Juan Moreno-Piraján:** Writing – original draft, Supervision, Methodology, Conceptualization. **Jarosław Serafin:** Writing – review & editing, Writing – original draft, Visualization, Validation, Project administration, Formal analysis, Data curation. **Rocío Sierra-Ramírez:** Supervision, Data curation, Conceptualization. **Ghualm Farid:** Writing – original draft. **Bartosz Dziejarski:** Writing – review & editing, Writing – original draft, Visualization, Validation, Formal analysis, Data curation. **Liliana Giraldo:** Writing – original draft, Supervision, Methodology, Conceptualization.

Declaration of Competing Interest

The authors declare that they have no known competing financial interests or personal relationships that could have appeared to influence the work reported in this paper.

Data availability

Data will be made available on request.

Acknowledgement

This research was supported by Apoyo Financiero para Doctorados de la Universidad de Los Andes. Also, the authors acknowledge the framework agreement between Universidad Nacional de Colombia and Universidad de los Andes (Bogotá, Colombia) under which this work was carried out. Professor Juan Carlos Moreno-Piraján also thanks for the grant to the Facultad de Ciencias of Universidad de los Andes, number INV-2023–1622735.

References

[1] B. Dziejarski, R. Krzyżyńska, K. Andersson, Current status of carbon capture, utilization, and storage technologies in the global economy: a survey of technical assessment, Fuel 342 (2023) 127776.
[2] J. NOAA, Carbon dioxide now more than 50 % higher than pre-industrial levels, Natl. Ocean. Atmos. Adm. (2022).
[3] V.G. Azevedo, S. Sartori, L.M. Campos, CO_2 emissions: a quantitative analysis among the BRICS nations, Renew. Sustain. Energy Rev. 81 (2018) 107–115.
[4] M. Crippa, G. Oreggioni, D. Guizzardi, M. Muntean, E. Schaaf, E. Lo Vullo, E. Solazzo, F. Monforti-Ferrario, J.G. Olivier, E. Vignati, Fossil CO_2 and GHG Emissions of All World Countries, Publication Office of the European Union, Luxemburg, 2019.
[5] B. Ekwurzel, J. Boneham, M.W. Dalton, R. Heede, R.J. Mera, M.R. Allen, P. C. Frumhoff, The rise in global atmospheric CO_2, surface temperature, and sea level from emissions traced to major carbon producers, Clim. Change 144 (2017) 579–590.
[6] M.V.N.L. Chaitanya, S. Arora, R.S. Pal, H.S. Ali, B.M. El Haj, R. Logesh, Assessment of Environmental Pollutants for Their Toxicological Effects of Human and Animal Health. Organic Micropollutants in Aquatic and Terrestrial Environments, Springer, Cham, 2024, pp. 67–85 (Nature Switzerland).
[7] M.M. Rahman, A.K. Mohanty, M.H. Rahman, Renewable energy, forestry, economic growth, and demographic impact on carbon footprint in India: does forestry and renewable energy matter to reduce emission? J. Environ. Stud. Sci. (2024) 1–13.
[8] M. Wang, A.S. Joel, C. Ramshaw, D. Eimer, N.M. Musa, Process intensification for post-combustion CO2 capture with chemical absorption: a critical review, Appl. Energy 158 (2015) 275–291.
[9] J. Serafin, B. Dziejarski, Activated carbons—Preparation, characterization and their application in CO2 capture: a review. Environ. Sci. Pollut. Res. (2023) 1–55.
[10] D.P. Vargas, L. Giraldo, J. Moreno, -Piraján, CO2 adsorption on granular and monolith carbonaceous materials, J. Anal. Appl. Pyrolysis 96 (2012) 146–152.
[11] S. Acevedo, L. Giraldo, J.C. Moreno-Piraján, Adsorption of CO2 on activated carbons prepared by chemical activation with cupric nitrate, ACS Omega 5 (2020) 10423–10432.
[12] M.S. Shafeeyan, W.M.A.W. Daud, A. Houshmand, A. Arami-Niya, Ammonia modification of activated carbon to enhance carbon dioxide adsorption: effect of pre-oxidation, Appl. Surf. Sci. 257 (2011) 3936–3942.
[13] B. Mousazadeh, N. Mohammadi, M.R. Khosravi-Nikou, Synthesis and characterization of porous activated carbons derived from lotus nut and their performance for CO2 adsorption, Int. J. Environ. Sci. Technol. 21 (6) (2024) 5379–5394.
[14] J. Serafin, M. Ouzzine, O.F.C. Junior, J. Sreńscek-Nazzal, Preparation of low-cost activated carbons from amazonian nutshells for CO2 storage, Biomass-.-. Bioenergy 144 (2021) 105925.
[15] J. Serafin, K. Kishibayev, R. Tokpayev, T. Khavaza, A. Atchabarova, Z. Ibraimov, J. C. Moreno-Piraján, Functional activated biocarbons based on biomass waste for CO2 capture and heavy metal sorption, ACS Omega 8 (50) (2023) 48191–48210.
[16] D. Panda, E.A. Kumar, S.K. Singh, Introducing mesoporosity in zeolite 4A bodies for Rapid CO2 capture, J. CO2 Util. 40 (2020) 101223.
[17] M.R. Zaeri, F. Esmaeilzadeh, Performance evaluation of static and dynamic CO2 adsorption from synthetic gas condensates using zinc oxide, silicon dioxide and zeolite 13X, Korean J. Chem. Eng. (2024) 1–14.
[18] W.-J. Son, J.-S. Choi, W.-S. Ahn, Adsorptive removal of carbon dioxide using polyethyleneimine-loaded mesoporous silica materials, Microporous Mesoporous Mater. 113 (2008) 31–40.
[19] H. Sui, F. Zhang, L. Zhang, D. Wang, Y. Wang, Y. Yang, J. Yao, Competitive sorption of CO2/CH4 and CO2 capture on modified silica surfaces: a molecular simulation, Sci. Total Environ. 908 (2024) 168356.
[20] V. Kulkarni, J. Parthiban, S.K. Singh, Direct CO2 capture from simulated and Ambient Air over aminosilane-modified hierarchical silica, Microporous Mesoporous Mater. 368 (2024) 112998.
[21] J. Yang, Y. Wang, L. Li, Z. Zhang, J. Li, Protection of open-metal V (III) sites and their associated CO2/CH4/N2/O2/H2O adsorption properties in mesoporous V-MOFs, J. Colloid Interface Sci. 456 (2015) 197–205.
[22] Y. Zhang, D. Zhang, P. Lei, Z. Yang, Z. Zhang, Synthesis of Ca-based metal–organic frameworks from carbide slag for CO2 adsorption. Sep. Purif. Technol. 335 (2024) 126247.
[23] H.N. Nguyen, T.P. Nguyen, P.T. Le, Q.M. Tran, T.H. Do, T.D. Nguyen, T.M.T. Dinh, Investigation on cost-effective composites for CO2 adsorption from post-gasification residue and metal organic framework, J. Environ. Sci. 148 (2025) 174–187.
[24] L. Wang, W. Xie, G. Xu, S. Zhang, C. Yao, Y. Xu, Synthesis of thiophene-based conjugated microporous polymers for high iodine and carbon dioxide capture, Polym. Adv. Technol. 33 (2022) 584–590.
[25] G. Singh, K.S. Lakhi, S. Sil, S.V. Bhosale, I. Kim, K. Albahily, A. Vinu, Biomass derived porous carbon for CO2 capture, Carbon 148 (2019) 164–186.
[26] J. Serafin, B. Dziejarski, J. Sreńscek-Nazzal, An innovative and environmentally friendly bioorganic synthesis of activated carbon based on olive stones and its potential application for CO2 capture, Sustain. Mater. Technol. 38 (2023) e00717.
[27] A. Samsuri, F. Sadegh-Zadeh, B. Seh-Bardan, Characterization of biochars produced from oil palm and rice husks and their adsorption capacities for heavy metals, Int. J. Environ. Sci. Technol. 11 (2014) 967–976.
[28] B.F.M.L. Gomes, S.V. Júnior, L.V.A. Gurgel, Production of activated carbons from technical lignin as a promising pathway towards carbon emission neutrality for second-generation (2G) ethanol plants, J. Clean. Prod. (2024) 141648.
[29] G. Crini, E. Lichtfouse, L.D. Wilson, N. Morin-Crini, Conventional and non-conventional adsorbents for wastewater treatment, Environ. Chem. Lett. 17 (2019) 195–213.
[30] K.T. Klasson, C.A. Ledbetter, M. Uchimiya, I.M. Lima, Activated biochar removes 100 % dibromochloropropane from field well water, Environ. Chem. Lett. 11 (2013) 271–275.
[31] J. Sreńscek-Nazzal, A. Kamińska, J. Serafin, B. Michalkiewicz, Chemical activation of banana peel waste-derived biochar using KOH and urea for CO2 capture, Materials 17 (4) (2024) 872.
[32] P. Kumar, S.N. Omer, M. Reddy, P. Saravanan, R. Rajeshkannan, M. Rajasimman, Y. Vasseghian, Exploring the role of activated charcoal from lignocellulosic biomass wastes for environmental pollution control, J. Energy Inst. (2024) 101626.
[33] X. Zhong, C. Li, L. Zhang, S. Zhang, Y. Wang, S. Hu, X. Hu, Bio-oil as a filler for enhancing development of micropores in activation of chicken bone, J. Environ. Chem. Eng. (2024) 112155.
[34] G. Jolly, L. Dupont, M. Aplincourt, J. Lambert, Improved Cu and Zn sorption on oxidized wheat lignocellulose, Environ. Chem. Lett. 4 (2006) 219–223.
[35] G. Ramalingam, A.K. Priya, L. Gnanasekaran, S. Rajendran, T.K. Hoang, Biomass and waste derived silica, activated carbon and ammonia-based materials for energy-related applications–A review, Fuel 355 (2024) 129490.
[36] M.J. Prauchner, K. Sapag, F. Rodríguez-Reinoso, Tailoring biomass-based activated carbon for CH4 storage by combining chemical activation with H3PO4 or ZnCl2 and physical activation with CO2, Carbon 110 (2016) 138–147.
[37] AGROSAVIA, "El Marañón, Una Excelente Proyección Para El Campo," 2022. ⟨https://www.agrosavia.co/noticias/el-maranon-cultivo-y-agronegocio-con-una-excelente-proyeccion-para-el-desarrollo-del-campo-colombiano⟩ (accessed Sep. 11, 2022).
[38] P. Das, A. Ganesh, Bio-oil from pyrolysis of cashew nut shell—a near fuel, Biomass-.-. Bioenergy 25 (2003) 113–117.
[39] V. Jiménez, A. Ramírez-Lucas, J.A. Díaz, P. Sánchez, A. Romero, CO2 capture in different carbon materials, Environ. Sci. Technol. 46 (13) (2012) 7407–7414.

[40] J. Serafin, B. Dziejarski, Activated carbons—preparation, characterization and their application in CO2 capture: a review. Environ. Sci. Pollut. Res. (2023) 1–55.
[41] F. Wu, H. Zhang, W. Liu, Q. Zhang, Q. Li, S. Zheng, P. Li, Transformation process of boehmite to γ-Al2O3 induced by high-energy ball milling, CrystEngComm (2024).
[42] G. Conte, A. Policicchio, M. Idrees, G. Desiderio, R.G. Agostino, Tuning the ultra-microporosity in hierarchical porous carbons derived from amorphous cellulose towards a sustainable solution for hydrogen storage, Int. J. Hydrog. Energy 50 (2024) 763–773.
[43] J.R. Li, J. Yu, W. Lu, et al., Porous materials with pre-designed single-molecule traps for CO2 selective adsorption, Nat. Commun. 4 (2013) 1538, https://doi.org/10.1038/ncomms2552.
[44] D. Lozano-Castelló, D. Cazorla-Amorós, A. Linares-Solano, Usefulness of CO2 adsorption at 273 K for the characterization of porous carbons, Carbon 42 (7) (2004) 1233–1242.
[45] F. Dai, Q. Zhuang, G. Huang, H. Deng, X. Zhang, Infrared Spectrum Characteristics and Quantification of OH Groups in Coal, ACS Omega 8 (19) (2023 May 3) 17064–17076, https://doi.org/10.1021/acsomega.3c01336. PMID: 37214670; PMCID: PMC10193429.
[46] M.A.L. Diaz, G.M. Del Fueyo, M.M. Mendes, Cuticle chemistry of the cheirolepidiaceae frenelopsis teixeirae from the lower cretaceous of Portugal. A case of study using ATR-FTIR spectroscopy, Rev. Palaeobot. Palynol. *319* (2023) 105001.
[47] K.K. Kishibayev, J. Serafin, R.R. Tokpayev, T.N. Khavaza, A.A. Atchabarova, D. A. Abduakhytova, J. Sreńscek-Nazzal, Physical and chemical properties of activated carbon synthesized from plant wastes and shungite for CO2 capture, J. Environ. Chem. Eng. *9* (6) (2021) 106798.
[48] Seo Hui Kang, Ji. Su Chae, Jung-Min Choi, Yoon-Jung Shin, Jae-Won Lee, Yun Chan Kang, Kwang Chul Roh, Pore-tailoring of pruned fruit tree branch derived activated carbon with hierarchical micropore structure for non-aqueous supercapacitors, J. Energy Storage 56 (2022) 106098.
[49] Y.L. Zhao, X. Zhang, M.Z. Li, J.R. Li, Non-CO 2 greenhouse gas separation using advanced porous materials, Chem. Soc. Rev. (2024).
[50] H. Li, Y. Qi, J. Chen, M. Yang, H. Qiu, Development of amine-pillar [5] arene modified porous silica for CO2 adsorption, and CO2/CH4, CO2/N2 Sep. Sep. Purif. Technol. (2024) 126400.
[51] J. Serafin, B. Dziejarski, O.F.C. Junior, J. Sreńscek-Nazzal, Design of highly microporous activated carbons based on walnut shell biomass for H2 and CO2 storage, Carbon *201* (2023) 633–647.
[52] H. El Ouahabi, A. Elmouwahidi, L. Cano-Casanova, M.Á. Lillo-Ródenas, M. C. Roman-Martínez, A.F. Pérez-Cadenas, M. Khaddor, From nutshells to energy cells: pioneering supercapacitor electrodes via innovative argan nutshell activated carbon synthesis, J. Energy Storage *82* (2024) 110598.
[53] S. Harabi, S. Guiza, A. Álvarez-Montero, A. Gómez-Avilés, C. Belver, J. J. Rodríguez, J. Bedia, Adsorption of 2, 4-dichlorophenoxyacetic acid on activated carbons from macadamia nut shells, Environ. Res. (2024) 118281.
[54] Lyu, D., Märker, K., Zhou, Y., Zhao, E.W., Gunnarsdóttir, A., Niblett, S., … & Grey, C. (2024). Understanding Sorption of Aqueous Electrolytes in Porous Carbon by NMR spectroscopy.
[55] O.P. Murphy, M. Vashishtha, P. Palanisamy, K.V. Kumar, A review on the adsorption isotherms and design calculations for the optimization of adsorbent mass and contact time, ACS Omega *8* (20) (2023) 17407–17430.
[56] S. Kandaswamy, V.M. Swarupa, S. Sur, G. Choubey, Y. Devarajan, R. Mishra, Cashew nut shell oil as a potential feedstock for biodiesel production: an overview, Biotechnol. Bioeng. *120* (11) (2023) 3137–3147.
[57] N.M. Nurazzi, M.R.M. Asyraf, M. Rayung, M.N.F. Norrrahim, S.S. Shazleen, M.S. A. Rani, A.R. Shafi, H.A. Aisyah, M.H.M. Radzi, F.A. Sabaruddin, et al., Thermogravimetric analysis properties of cellulosic natural fiber polymer composites: a review on influence of chemical treatments, Polymers 13 (16) (2021) 2710, https://doi.org/10.3390/polym13162710.
[58] E. Papadopoulou, K. Chrissafis, Thermal study of phenol–formaldehyde resin modified with cashew nut shell liquid. Thermochim. Acta *512* (1-2) (2011) 105–109.
[59] O.F. Cruz Jr, J. Serafin, F.Z. Azar, M.E. Casco, J. Silvestre-Albero, D. Hotza, C. R. Rambo, Microwave-assisted hydrothermal carbonization and characterization of Amazonian biomass as an activated carbon for methane adsorption, Fuel 358 (2024) 130329.
[60] P. Mehra, A. Paul, Decoding carbon-based materials' properties for high CO2 capture and selectivity, ACS Omega 7 (38) (2022 Sep 13) 34538–34546, https://doi.org/10.1021/acsomega.2c04269. PMID: 36188328; PMCID: PMC9520712.
[61] J. Serafin, B. Dziejarski, O.F.C. Junior, J. Sreńscek-Nazzal, Design of highly microporous activated carbons based on walnut shell biomass for H2 and CO2 storage, Carbon 201 (2023) 633–647.
[62] S. Garg, P. Das, Microporous carbon from cashew nutshell pyrolytic biochar and its potential application as CO2 adsorbent, Biomass-.-. Convers. Biorefin 10 (2020) 1043e61.
[63] G. Singh, K.S. Lakhi, K. Ramadass, S. Kim, D. Stockdale, A. Vinu, A combined strategy of acid-assisted polymerization and solid state activation to synthesize functionalized nanoporous activated biocarbons from biomass for CO2 capture, Microporous Mesoporous Mater. 271 (2018) 23–32.
[64] C. Zhang, W. Song, Q. Ma, L. Xie, X. Zhang, H. Guo, Enhancement of CO2 capture on biomass-based carbon from black locust by KOH activation and ammonia modification, Energy Fuels 30 (5) (2016) 4181–4190.
[65] W. Travis, S. Gadipelli, Z. Guo, Superior CO2 adsorption from waste coffee ground derived carbons, RSC Adv. 5 (37) (2015) 29558–29562.
[66] A.S. Ello, L.K. de Souza, A. Trokourey, M. Jaroniec, Coconut shell-based microporous carbons for CO2 capture, Microporous Mesoporous Mater. 180 (2013) 280–283.
[67] W. Sangchoom, R. Mokaya, Valorization of lignin waste: carbons from hydrothermal carbonization of renewable lignin as superior sorbents for CO2 and hydrogen storage, ACS Sustain. Chem. Eng. 3 (7) (2015) 1658–1667.
[68] H.M. Coromina, D.A. Walsh, R. Mokaya, Biomass-derived activated carbon with simultaneously enhanced CO 2 uptake for both pre and post combustion capture applications, J. Mater. Chem. A 4 (1) (2016) 280–289.
[69] Y. Li, G. Ruan, A.S. Jalilov, Y.R. Tarkunde, H. Fei, J.M. Tour, Biochar as a renewable source for high-performance CO2 sorbent, Carbon 107 (2016) 344–351.
[70] D.P. Vargas, L. Giraldo, J.C. Moreno-Piraján, Carbon dioxide and methane adsorption at high pressure on activated carbon materials, Adsorption 19 (2013) 1075–1082.
[71] D.C. Azevedo, J.C.S. Araújo, M. Bastos-Neto, A.E.B. Torres, E.F. Jaguaribe, C. L. Cavalcante, Microporous activated carbon prepared from coconut shells using chemical activation with zinc chloride, Microporous Mesoporous Mater. 100 (1-3) (2007) 361–364.
[72] F. Oguz Erdogan, A comparative study on methane adsorption onto various adsorbents including activated carbons, zeolites, MWCNT, and MCM-41, Int. J. Coal Prep. Util. 42 (7) (2022) 2078–2098.
[73] N. Bagheri, J. Abedi, Adsorption of methane on corn cobs based activated carbon, Chem. Eng. Res. Des. 89 (10) (2011) 2038–2043.
[74] M.E. Casco, M. Martínez-Escandell, E. Gadea-Ramos, K. Kaneko, J. Silvestre-Albero, F. Rodríguez-Reinoso, High-pressure methane storage in porous materials: are carbon materials in the pole position? Chem. Mater. 27 (3) (2015) 959–964.
[75] A.L. Myers, J.M. Prausnitz, Thermodynamics of mixed-gas adsorption, AIChE J. 11 (1) (1965) 121–127.
[76] R.B. Rios, F.M. Stragliotto, H.R. Peixoto, A.E.B. Torres, M. Bastos-Neto, D.C. S. Azevedo, C.L. Cavalcante Jr, Studies on the adsorption behavior of CO2-CH4 mixtures using activated carbon, Braz. J. Chem. Eng. 30 (2013) 939–951.
[77] F. Dreisbach, R. Staudt, J.U. Keller, High pressure adsorption data of methane, nitrogen, carbon dioxide and their binary and ternary mixtures on activated carbon, Adsorption 5 (1999) 215–227.
[78] R.P. Ribeiro, T.P. Sauer, F.V. Lopes, R.F. Moreira, C.A. Grande, A.E. Rodrigues, Adsorption of CO2, CH4, and N2 in activated carbon honeycomb monolith, J. Chem. Eng. Data 53 (10) (2008) 2311–2317.
[79] M. Heuchel, G.M. Davies, E. Buss, N.A. Seaton, Adsorption of carbon dioxide and methane and their mixtures on an activated carbon: simulation and experiment, Langmuir 15 (25) (1999) 8695–8705.
[80] B. Yuan, X. Wu, Y. Chen, J. Huang, H. Luo, S. Deng, Adsorption of CO2, CH4, and N2 on ordered mesoporous carbon: approach for greenhouse gases capture and biogas upgrading, Environ. Sci. Technol. 47 (10) (2013) 5474–5480.
[81] M.C. Castrillon, K.O. Moura, C.A. Alves, M. Bastos-Neto, D.C. Azevedo, J. Hofmann, R. Glaser, CO2 and H2S removal from CH4-rich streams by adsorption on activated carbons modified with K2CO3, NaOH, or Fe2O3, Energy Fuels 30 (11) (2016) 9596–9604.
[82] D. Peredo-Mancilla, C.M. Ghimbeu, B.N. Ho, M. Jeguirim, C. Hort, D. Bessieres, Comparative study of the CH4/CO2 adsorption selectivity of activated carbons for biogas upgrading, J. Environ. Chem. Eng. 7 (5) (2019) 103368.